Bioactive Materials 15 (2022) 330–342

Contents lists available at ScienceDirect

Bioactive Materials

journal homepage: www.keaipublishing.com/en/journals/bioactive-materials

N-carboxymethyl chitosan/sodium alginate composite hydrogel loading plasmid DNA as a promising gene activated matrix for in-situ burn wound treatment

Litong Wang [a,1], Le Sun [a,1], Zhiyang Gu [a], Wenya Li [a], Lili Guo [a], Saibo Ma [a], Lan Guo [a], Wangwang Zhang [a], Baoqin Han [a,b], Jing Chang [a,b,*]

[a] College of Marine Life Science, Ocean University of China, Qingdao, 266003, PR China
[b] Laboratory for Marine Drugs and Bioproducts, Pilot National Laboratory for Marine Science and Technology (Qingdao), Qingdao, 266235, PR China

ARTICLE INFO

Keywords:
Gene activated matrix
Hydrogel
Wounds healing
N-carboxymethyl chitosan
Sodium alginate

ABSTRACT

Improving the degree of vascularization through the regulation of wound microenvironment is crucial for wound repair. Gene activated matrix (GAM) technology provides a new approach for skin regeneration. It is a local gene delivery system that can not only maintain a moist environment, but also increase the concentration of local active factors. For this purpose, we fabricated the mVEGF165/TGF-β_1 gene-loaded *N*-carboxymethyl chitosan/sodium alginate hydrogel and studied its effect on promoting deep second degree burn wound repair. The average diameter of the hydrogel pores was 100 μm and the porosity was calculated as 50.9%. SEM and CLSM images showed that the hydrogel was suitable for cell adhesion and growth. The NS-GAM could maintain continuous expression for at least 9 days *in vitro*, showing long-term gene release and expression effect. Deep second-degree burn wound model was made on the backs of Wistar rats to evaluate the healing effect. The wounds were healed by day 22 in NS-GAM group with the prolonged high expression of VEGF and TGF-β_1 protein. A high degree of neovascularization and high expression level of CD34 were observed in NS-GAM group in 21 days. The histological results showed that NS-GAM had good tissue safety and could effectively promote epithelialization and collagen regeneration. These results indicated that the NS-GAM could be applied as a promising local gene delivery system for the repair of deep second-degree burn wounds.

1. Introduction

The skin is the outermost covering and one of the most important organs of the human body, and it has a variety of physiological functions [1]. In particular, it plays an important role in protecting the human body from the external environment [2]. The injury of the skin may cause the lack of physiological homeostasis of the whole body [3]. According to the World Health Organization, burn wounds have increased dramatically in the past decade, killing about 180,000 people worldwide each year, with the majority of these burn cases occurring in low- and middle-income countries [4]. The main differences between burns and cuts are the severe inflammatory infiltration caused by the inflammatory response after a burn, the pain caused by the burn, the immediate loss of blood flow to the site of the injury, and the changes in blood flow to the surrounding area. These negative effects can cause the healing difficulty of the injured wounds or the formation of the scars [5–8].

According to the depth of the burn sites, burn wounds are classified into three categories burn wounds: first-degree burn wounds (superficial), second-degree burn wounds (partial burn wounds) and third-degree burn wounds (full thickness burn wounds) [9]. After acute or chronic skin injury, the body initiates a four-stage process of hemostasis, inflammation, proliferation, and remodeling at the site of injury, during which the healed damaged tissue heals and rebuilds its barrier function [10,11]. The successful wounds healing requires appropriate therapy to regulate a complex set of interactions between different cell types, cytokine mediators, and extracellular matrix throughout the different stages of healing [12]. However, due to long-term treatment in some cases of major injuries, such as second or third degree burns, the natural

Peer review under responsibility of KeAi Communications Co., Ltd.
* Corresponding author. College of Marine Life Science, Ocean University of China, Qingdao, 266003, PR China.
E-mail address: changjing@ouc.edu.com (J. Chang).
[1] These two authors contributed equally to this work.

https://doi.org/10.1016/j.bioactmat.2021.12.012
Received 4 October 2021; Received in revised form 4 December 2021; Accepted 9 December 2021
Available online 20 December 2021

process of wounds healing is not satisfying, resulting in physical and psychological trauma of patients and chronic disability, which seriously affects the quality of life of patients or even becomes an important cause of morbidity or death [13–15]. The gold standard for burn treatment is the use of autografts. However, the limited skin donor sites and high risk of infection limit the use of autografts, requiring the alternatives to facilitate burn wounds coverage and healing [16].

Studies have shown that the wound dressings play a key role in the management of local burn wounds by creating a favorable environment for reepithelialization [17]. The ideal wound dressing should have a number of characteristics, such as maintaining a moist wound healing environment, being non-sensitive and non-toxic, facilitating gas exchange, absorption of wound exudates, preventing further trauma/infection, and infrequent dressing changes that facilitate epithelial cell migration across the wound beds [18,19]. Hydrogels are three-dimensional cross-linked polymers that can absorb water and have a flexible porous structure, which meet many requirements for ideal wound dressings and are hereby the most common choice for wound dressings. The hydrogels could provide a dynamic balance between excess exudate, providing water to the wound while absorbing the exudate, protecting the wound from infection, and preventing dehydration and adhesion between the wounds and the dressings [20–22]. The high water content also promotes the transfer of water vapor and oxygen, and promotes cell metabolism, which could accelerate the healing while reducing damage to healing tissue after dressing removal. In addition, the hydrogels are regarded to have pain relief and cooling effects [23–25].

Because of the network structure of hydrogels, the hydrogels offer the possibility of loading and controlling the release of genes/drugs, forming in situ scaffolds loaded with active substances and helping to further facilitate treatment [26]. The traditional tissue engineering usually uses protein-like growth factors, but there are problems such as easy degradation, unstable biological activity *in vivo*, systemic toxicity caused by explosive release and high cost [27,28]. Therefore, Bonadio Group initially suggested using the growth factor gene instead of the corresponding protein to eliminate these problems mentioned above [29]. Gene activated matrix (GAM) can be formed by adding gene carrier loaded plasmid to hydrogel scaffold [30]. The GAM can deliver genes directly to the target, achieving high in situ vector concentrations, prolongating in situ tissue contact, and avoiding many systemic problems of gene delivery, such as enzyme degradation and immune effects. The GAM, which combines tissue engineering with gene therapy, has attracted increasing attention due to its advantages in local delivery and expression, as well as its efficiency in local therapy [31,32].

The materials of hydrogels were mainly divided into two categories: synthetic materials and natural materials. Synthetic polymer materials usually had good mechanical properties, but poor biocompatibility and safety, and they were lack of cell-induced activity. Compared with synthetic polymers, natural materials could provide more effectively support for cell viability, migration, adhesion, and differentiation, mimicking the mechanical and biochemical properties of the natural environment, and reducing the side effects of polymer degradation [33,34]. In this study, chitosan and alginate were used to construct the hydrogel, which were two attractive materials with excellent biocompatibility, biodegradability, and bioactivity for wound beds healing. Chitosan is a cationic polysaccharide composed of *N*-glucosamine and *N*-acetyl-glucosamine units, with the sugar backbone linked by β-1, 4-glucosidic bonds [35,36]. The wound-healing applications of chitosan and its derivatives have been reported by several literatures [37]. However, the poor solubility in aqueous solution and organic solvents limited its applications. In order to overcome the poor solubility of chitosan, *N*-carboxymethylation was used to modify chitosan [38,39]. A new water-soluble chitosan derivative of *N*-carboxymethyl chitosan (NCMC) was received [40]. Sodium alga acid (SA) is obtained from the cell walls of brown algae, which is a linear block polysaccharide composed of *α*-L-mannuronic acid and *β*-D-guluronic acid units, linked by (1–4)-linkages [41]. However, the NCMC alone has poor mechanical properties and easy to swell, while the SA used alone is very brittle and has poor water resistance, showing seldom bacteriostatic effect. Using either component of chitosan and sodium alginate alone was not ideal for skin wound dressings. The combination of these two materials could make up the deficiency of single component, providing satisfactory performance and wide application. A stable hydrogel was achieved via the response of NCMC and SA in an electric neutral condition.

Two other important factors in GAM are therapeutic plasmids and gene vectors. Vascular endothelial growth factor (VEGF) is an essential factor for the revascularization, which is important for the healing of wound repair [42,43]. TGF-β_1 is another important growth factor for wound repair [44]. The main function of TGF-β_1 is promoting proliferation and differentiation of the fibroblasts in wound beds, which is helpful for the collagen neogenesis. Some positive results with injection of VEGF and TGF-β_1 plasmids have been received in wound repair clinical trials for leg ischemia, diabetes mellitus ulcer, and coronary artery disease [45–47]. Two new VEGF and TGF-β_1 plasmids with effective promoters to enhance the expression of VEGF and TGF-β_1 were constructed by our lab. To mimic the main components of viral envelopes which are composed of peptides and polysaccharides, an arginine modified chitosan was synthesized and it is expected as a gene vector in GAM for wound healing [48].

Herein, a novel type of GAM for deep second-degree burn wound healing was constructed, which had three key elements, including *N*-carboxymethyl chitosan/sodium alginate hybrid scaffold, efficient gene vector used of arginine modified chitosan (Arg-CS), and high-expressed therapeutic plasmids. The plasmids/Arg-CS complexes were loaded in the *N*-carboxymethyl chitosan/sodium alginate composite scaffold for GAM fabrication (see Scheme 1). In order to evaluate the in situ repair effect of NS-GAM on wound healing, a deep second degree burn model was used. The GAM was expected to produce a satisfying and long-term expression of growth factors to promote the healing of deep second-degree burn wound.

2. Materials and methods

2.1. Materials

The *N*-carboxymethyl chitosan derivative (NCMC, Mn = 150 kDa, deacetylation degree of 90%) and the arginine modified chitosan (Arg-CS, Mn = 20 kDa) were synthesized by our lab according to the methods previously reported [40,48]. Dulbecco's Modified Eagles Medium (DMEM) and Fetal Bovine Serum (FBS) were purchased from Hyclone (USA). LDH Cytotoxicity Assay Kit (Beyotime Institute of Biotechnology, China), cell lysate and the luciferase reporter gene assay kit were purchased from Promega (USA). ELISA Kits of TGF-β_1 and VEGF were purchased from RND Semicon Co. Ltd. (Korea). BCA protein assay kits were purchased from Pierce (USA). Masson's Trichrome staining were purchased from MD Chemicals Inc., (USA). All other chemicals were reagent grade and used as received.

NIH3T3 cell line was purchased from Institute of Biochemistry and Cell Biology, SIBS, CAS (China). Adult male Sprague-Dawley (SD) rats weighing 200 ± 20 g and were supplied by the Laboratory Animal Center of Shanxi Medical University in China, with certificate of SCXK (Jin) 20150001. All animals were kept under a 12 h light-dark cycles at consistent temperature (25 ± 3 °C) and relative humidity (60–70%). Experiments were performed in accordance with the ethical guidelines of the Shandong Province Experimental Animal Management Committee and were in complete compliance with the National Institutes of Health Guide for the Care and Use of Laboratory Animals.

2.2. Preparation and characterization of NCMC/SA scaffolds

A stock solution of NCMC (3%, w/v) was prepared by dissolving NCMC in deionized water and stirring to dissolve at room temperature.

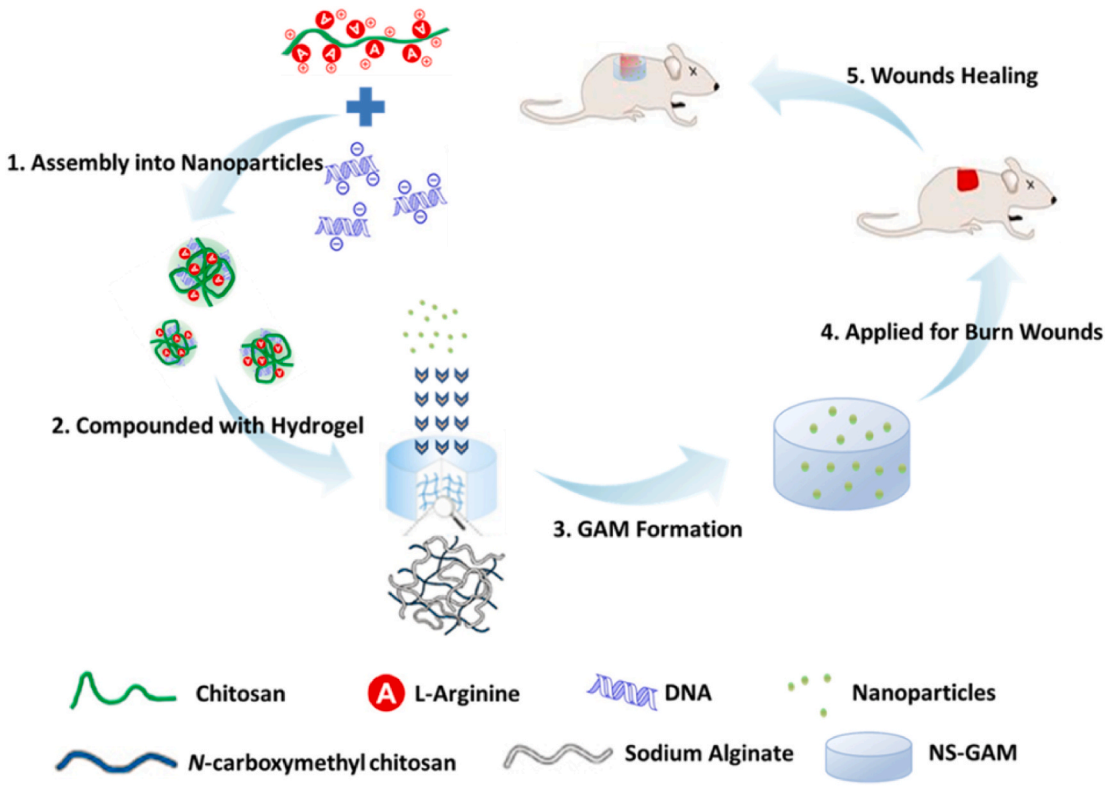

Scheme 1. Schematic illustration of NS-GAM as a gene delivery system for deep second-degree burn wound.

Subsequently, the same amount of SA (3%, w/v) was acquired by the same method. The dissolved NCMC and SA solutions were blended with different volume ratio (1:9, 3:7, 5:5, 7:3, 9:1), named NS1, NS2, NS3, NS4, and NS5. The solutions were sonicated to remove the trapped air bubbles. After thoroughly stirring, the air bubble-free solutions were poured into shallow dishes (with a diameter of 3 cm). The solution was then frozen at −20 °C for 24 h and was subsequently lyophilized in a freeze drier. The freeze-dried samples were cross-linked with 1% $CaCl_2$ solution for 12 h. The cross-linked NCMC/SA scaffolds were thoroughly rinsed with deionized water to remove residual $CaCl_2$ and kept at −20 °C for 24 h and again lyophilized. The morphologies of NCMC/SA scaffolds were observed by SEM (Hitachi S–3400N, Japan), the porosity and water content were calculated. The chemical structure of NCMC/SA hydrogel was characterized by Fourier Transform Infrared Spectra (FTIS, Thermo Scientific Nicolet Nexus-470). Rheological tests on NCMC/SA hydrogel were performed using a Thermo scientific Haake MARS III (USA) in a cone-plate mode (cone angle, 2.0°; plate diameter 34.995 mm, truncation 0.105 mm) at 25 °C. After the linear viscoelastic regime was determined by strain sweeping from 0.01 to 100% strain at 1 Hz, dynamic frequency sweeps were carried out from 0.01 to 10 Hz oscillation at 1% strain. The thermal property was investigated using thermogravimetric analysis (TGA). The TGA analysis was carried out on a thermogravimetric analyzer (Mettler Toledo TGA/DSC3+, Swiss) with a heating rate of 10 °C min^{-1} from room temperature to 700 °C under dry nitrogen atmosphere at a flow rate of 50 mL/min. The static contact angles (Solon tech.SL200B, China) were measured between the drop of fluid and the hydrogel surface to identify the hydrophilicity. The phosphate buffer saline (PBS, pH 7.4) was used to measure the contact angle on the samples with a 5 μL drop.

2.3. Cytotoxicity of NCMC/SA scaffolds

The evaluation of the cytotoxicity of NCMC/SA scaffold was performed by MTT assay. The leaching liquor of the NCMC/SA scaffold was prepared according to the ISO 10993-5 standards. NIH3T3 cells were seeded on 96-well plates with an initial density of 4×10^4 cells/cm^2 and cultured in Dulbecco's minimal essential medium (DMEM) supplemented with 10% heat-inactivated fetal bovine serum (FBS) and antibiotics (100 U/ml penicillin G and 100 mg/mL streptomycin) at 37 °C under an atmosphere of 5% CO_2 in air and 100% relative humidity. After incubated for 24 h, the cells were treated with the leaching liquor at different concentrations of 100%, 50% and 25%. After incubated for another 24 and 48 h, a 3-(4,5-dimethylthiazol-2-yl)-2,5-diphenyl tetrazolium bromide (MTT) test was carried out to quantify the viability of the cells. Briefly, 20 μL of MTT solution dissolved in PBS (5 mg/mL) was added to each well and further incubated for 4 h. The medium was then replaced with 150 μL DMSO to dissolve the formazan crystals. After gently agitated for 5 min, the absorbance at 570 nm was measured using a Thermo Varioskan Flash microplate reader. The cells in culture plate were used as control. The relative cell viability was measured as the formula below:

$$\text{Cell viability (\%)} = (\text{OD sample})/(\text{OD control}) \times 100\%$$

2.4. The 3D cell culture on the NCMC/SA scaffold

NIH3T3 cells were seeded on NCMC/SA scaffold in 24-well plates at a density of 4×10^4 cells/cm^2 and cultured in the same condition described above. After incubated for 24 and 48 h, a lactate dehydrogenase (LDH) test was carried out to quantify the viability of the cells by a LDH Assay Kit. Part of the scaffolds were washed gently by PBS, dehydrated and dried by CO_2 critical-point drying method. Then the morphology of the scaffold surface was observed by SEM (Hitachi S–3400 N, Japan). Another part of the scaffolds were also washed gently by PBS and used for further observation of the NIH3T3 cells. The cells cultured in the scaffold were stained with Hoechst 33258 according to the manufacturer's protocol and observed by a Confocal Laser Scanning Microscopy (Leica TCS SP5, Germany).

2.5. Preparation of NS-GAM and in vitro release study

The NCMC/SA Gene Active Matrices (NS-GAM) were prepared with the addition of Arg-CS/pDNA complexes into NCMC/SA scaffolds. Briefly, the Arg-CS/pDNA nanoparticles with the N/P ratio of 45 were prepared according to the method reported before [48]. NCMC/SA scaffold with the weight of 10 mg was immersed into 600 μL Arg-CS/pDNA nanoparticles solution (containing 800 μg pDNA) at 4 °C for 24 h. The immersed NCMC/SA scaffold was taken out of the solution and rinsed gently with 500 μL PBS twice. For each time the scaffold was rinsed for 5 min to remove the free nanoparticles. The maximum loading content of the nanoparticles in NCMC/SA scaffold was calculated by subtracting the retained nanoparticles in the solution and rinsed PBS. The rinsed NS-GAM was put into different PBS (pH = 7.2, 5.0 and 1.45) at 4 °C for the next 20 days and 5 μL of solution was taken out of the release medium and replaced with the same volume of fresh PBS solution for each day. The pDNA content released was measured by a Nanodrop (Nanodrop 2000, Thermo Scientific). The morphology of NS-GAM was also observed by SEM (Hitachi S–3400 N, Japan). After 20 days, the final release Arg-CS/pDNA complexes in pH7.2 buffer was collected, freeze-dried and dissolved with PBS into a 2 mg/mL solution. 5 μL SDS (10%w/v), 0.5 μL EDTA (0.5 M) and 4.5 μL heparin sodium injection were added to each 10 μL solution, which were incubated at 37 °C for 2 h to completely dissociate the DNA from the Arg-CS/pDNA complexes. The integrity of the plasmid in 6 parallel samples was determined by agarose gel electrophoresis with 1% (w/v) agarose gel at 80 V for 70 min.

2.6. In vitro gene transfection of NS-GAM

To evaluate the *in vitro* transfection efficiency of the Arg-CS/pDNA nanoparticles released from the NS-GAMs, the NIH3T3 cells were analyzed for green fluorescence protein (pEGFP-C1), luciferase (pGL3-Luc), VEGF (pcDNA3.1(+) - mVEGF165) and TGF-β_1 (pcDNA3.1(+) - TGF-β_1) expression. Briefly, the solutions with released Arg-CS/pDNA nanoparticles for 1, 3, 5, 7 and 9 days were used. NIH3T3 cells were seeded on 24-well plates with an initial density of 8×10^4 cells per well and incubated for 24 h. The solutions contained Arg-CS/pDNA nanoparticles were added into each well and incubated at 37 °C for 4 h in DMEM without FBS. The complexes were removed and the cells were incubated in fresh DMEM at 37 °C for another 48 h. The cells were analyzed for green fluorescence protein expression with a fluorescence microscope (Leica, Germany). The fluorescence intensity of GFP was also quantified by flow cytometry (FACS AriaTMII, BD, USA).

To assay the expression of luciferase, the medium was removed and the cells were rinsed gently with cold PBS and lysed using luciferase lysis buffer at the concentration of 200 μL/well. The cell suspension was subjected to freezing (−80 °C, 30 min) and thawing, and then centrifuged at 12,000 rpm for 3 min. The luciferase activity was measured by detecting the light emission from an aliquot of cell lysate incubated with 100 μL of luciferase substrate in a Thermo Varioskan Flash microplate reader. The relative light units (RLU) were normalized to protein concentrations in the cell extracts, which were measured using a bicinchoninic acid (BCA) protein assay kit. All the experiments were carried out in triplicate to ascertain the reproducibility.

To essay the expression of VEGF and TGF-β_1, the medium were collected and centrifuged at 10,000 rpm for 10 min at 4 °C to remove debris and insoluble materials. The supernatant was used for the test. The contents of VEGF and TGF-β_1 were determined by ELISA Kits (R&D Semicon Co. Ltd.) according to the manufacturer's protocol. The measurement of VEGF and TGF-β_1 were normalized to protein concentrations in the cell extracts, which were measured using a bicinchoninic acid (BCA) protein assay kit. All the experiments were carried out in triplicate to ascertain the reproducibility.

2.7. Histocompatibility and degradability of NS-GAM in vivo

The sterilized NS-GAMs (8 mm in diameter) were implanted into the back subcutaneous tissue of Wistar rats to evaluate the histocompatibility and degradability *in vivo*. Three rats were sacrificed on 3d, 9d, 15d, 21d, and 27d after the implantation. The membranes were retrieved, rinsed, dried and weighted to calculate the degradation rate. The surrounding tissues were removed, fixed with 4% neutrally buffered formaldehyde, embedded in paraffin, stained with hematoxylin-eosin (HE) and analyzed for histology.

2.8. Preparation of deep second-degree burn animal model

The animal experiment was approved by the ethics committee of Ocean University of China. In accordance to the guidelines, all animals received humane care during all steps of the experiments. The wound-healing efficacy of NS-GAM was evaluated using a rat model. 60 male Wistar rats with approximately 220 g weight were anesthetized by intraperitoneal injection of chloral hydrate at a dose of 350 mg/kg. The skin of the animal was shaved and disinfected using 70% ethanol. A cylindrical shaped tube with the diameter of 2.4 cm was placed on the back of rat, then hot water (95 °C) was poured into the tube and held for 15s. The deep second-degree burn wound was prepared and each rat has two wounds on the back.

2.9. The healing rate of NS-GAMs on deep second-degree burn wounds

The rates with deep second-degree burn wound were kept in separate cages and fed with commercial rat food and water till they were sacrificed. All wounded animals were randomly divided into two groups: control group and NS-GAM group. For the next 9 days, sterilized NS-GAM scaffolds were applied to the wound beds of NS-GAM group. The group of sterilized saline coated on the wound beds was used as control. The wounds were grossly examined and photographed for the measurement of healing rates of the wounds. The rats of each group sacrificed each time had 4 paralleled samples. Apart from the sacrificed rats, all the remaining rats were evaluated at each time point and the healing rate of the wounds was calculated using the equation below:

$$\text{Healing Rate (HR, \%)} = (A_0\text{-}A_t)/A_0 \times 100\%$$

Where A_0 and A_t were the initial wound area and the wound area after each interval time. The areas of the wounds were measured from the photographs using Image J software.

2.10. Pathological examination of the wounds

The rats were sacrificed on day 3, 12 and 21. The full thickness skin biopsies were harvested from the wound. The sections of healing wounds were fixed with 10% buffered formaldehyde, embedded in paraffin and sectioned. The sections were stained routinely with hematoxylin-eosin (HE) for histological assessment and Masson's Trichrome for collagen assessment.

2.11. Quantification of VEGF and TGF-β_1 of the wounds

The rats were sacrificed on day of 1, 3, 5, 7, 9, 12 and 15. The full thickness skin samples were obtained, weighted and homogenized in tissue lysate (100 mg/mL) with a tissue homogenizer (IKA, Germany). The homogenates were centrifuged at 10,000 rpm for 10 min at 4 °C twice to remove debris and insoluble materials. The supernatant was used for test. The contents of VEGF and TGF-β_1 were determined by ELISA Kits according to the manufacturer's protocol. The measurement of VEGF and TGF-β_1 were normalized to protein concentrations in the tissue extracts, which were measured using a bicinchoninic acid (BCA) protein assay kit. All the experiments were carried out in triplicate to

ascertain the reproducibility. The samples at 3, 7 and 12 days were also fixed and observed by TGF-β_1 and VEGF immunohistochemical method.

2.12. Neovascularization at the burn wounds

The blood flow velocity of the wounds was examined each day by a Laser Doppler Flowmetry (Sweden) and the average blood flow velocity was calculated by the LDF software. The samples of the wounds at 3, 7, 12 and 21 days were fixed and observed by CD 34 immunohistochemical method.

2.13. Statistical analysis

All data were expressed as means ± SD of a representative of several similar experiments. Statistical difference between several groups was evaluated via a one-way analysis of variance (ANOVA), and a value of $P < 0.05$ was considered significant (computed by SPSS version 13.0 Software).

3. Results and discussion

The photograph of NCMC/SA scaffolds was shown in Fig. 1 (A and B), which was a scaffold with short cylindrical shape and white color. The diameter of the scaffold was about 24 mm and the depth was about 6 mm. It could clearly be seen the surface of each sides of the scaffold was very smooth and glossy. The scaffold had ideal toughness, which was easy to be operated in its utilization. As shown in Fig. 1 (C and D), the porosity results showed that NS1 and NS5 had high porosity, both higher than 50%, while NS3 had a relatively low porosity of 43.17%. The results of water content were consistent with the results of porosity, and NS3 had the lowest water content. Due to the high water content and water absorption of NS1 and NS5, it was found that the NS1 and NS5 hydrogels dissociated and broke after a certain period of swelling, which were not suitable for subsequent application. Because the NCMC had been demonstrated good performance in promoting wound healing in our previous studies [40], in order to ensure as much proportion of NCMC as possible in hydrogels, NS4 hydrogel was selected for subsequent experiments. The morphologies of NS4 scaffolds were shown in Fig. 1 (E and F). It could be seen that some pores of the scaffolds were uniform and heading through, the average diameter of the pores was 100 μm. The porosity of the scaffolds was calculated as 50.9%.

The pore size and porosity had important influence on the mechanical properties and drug release ability of the hydrogels [49,50]. With the increase of the pore size and porosity, more water molecules entered into the network of the hydrogel, which could accelerate the swelling rate of the hydrogel, increase the drug loading efficiency. However, the drug release speed could be accelerated, which reduced the ability of the hydrogel to control release. On the contrary, if the pore size and porosity were small, the tight gel network could hinder the diffusion of the water molecules, which leaded to the weak moisturizing ability. From the aspect of the mechanical strength of the hydrogel, the decrease of pore size could make the structure get close and increase the gel strength. In this case, little deformation of the hydrogel happened under external force. The pore size of hydrogel was also very important for angiogenesis [51–53]. Too small pore size could limit the migration and proliferation of the cells. When the pore size was less than 50 μm, cells and new blood vessels were limited to the surface of the hydrogel and could not enter into the internal of the hydrogel. When the pore size of the scaffold was greater than 50 μm, it allowed the diffusion of nutrients and oxygen, meanwhile allowing the expulsion of metabolites. Materials with pore sizes greater than 100 μm showed ideal vascularization. However, too large of the pore size was not suitable for the hydrogel. Studies had shown that when the pore size was greater than 400 μm, the degree of vascularization could not increase anymore, and the excessive pore size could reduce the mechanical properties of the hydrogel. In addition, the connectivity and uniform distribution of the pores were also key factors affecting vascularization. The average diameter of the pores was 100 μm and the porosity of the scaffolds was calculated as 50.9% in NCMC/SA hydrogel, which matched the properties of hydrogels that could well promote angiogenesis.

As shown in Fig. 2 (A), the infrared absorption band was the O–H and N–H stretching vibration peaks of NCMC in the range of 3000 cm^{-1} to 3700 cm^{-1}. The red shift of the spectral band here indicated that N–H on NCMC was acylated and the hydrogen bonding of molecules was reduced. In the range of 2840 cm^{-1}-2962cm^{-1}, it was the stretching vibration peak of various CH, CH_2 and CH_3, the absorption peak at 2926 cm^{-1} was the antisymmetric stretching vibration peak of CH_2, and the wide peak at 1598 cm^{-1} was caused by the asymmetric stretching vibration of primary amide of NCMC. The narrow peak at 1417 cm^{-1} was caused by the C═O symmetric stretching of SA, the characteristic peak at 1114 cm^{-1} was caused by C–N in NCMC, and the absorption peak at 1036 cm^{-1} was caused by the C–O stretching vibration of SA. Polymer materials were typical viscoelastic materials and showed dynamic viscoelastic under the alternating stress. The storage modulus (G′) and loss modulus (G″) were two important viscoelastic parameters. Fig. 2 (B) showed the rheological properties of NCMC/SA hydrogel. It could be seen that the storage moduli of the hydrogel were slightly higher than the loss moduli, which demonstrated the hydrogel was in a typical gel state. The value of G′ and G″ of the hydrogel varied from 10,000 to 40,000 Pa. Compared with the hydrogels prepared by natural polymers

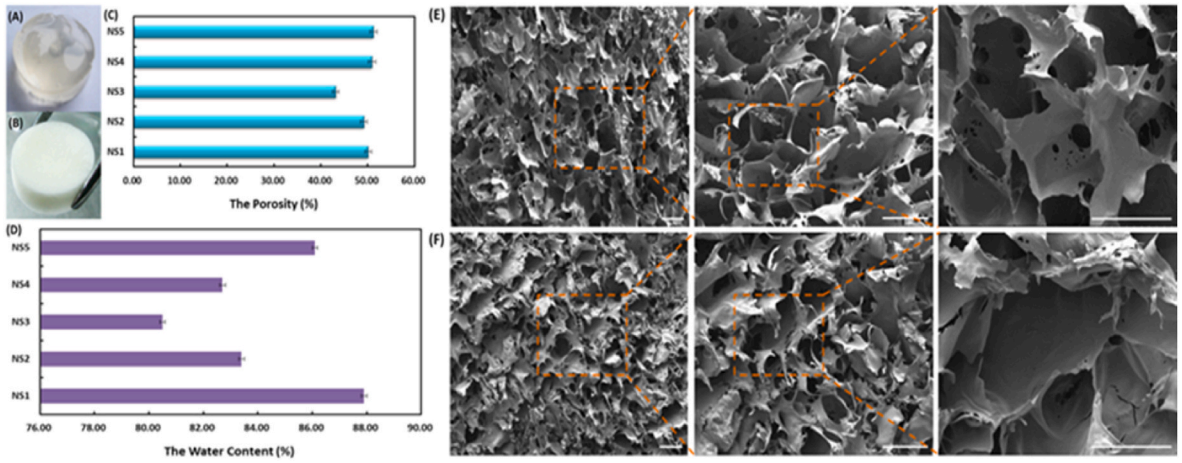

Fig. 1. The hygrometric state (A) and dry state (B) of NCMC/SA scaffolds; (C) The porosity of NCMC/SA scaffolds; (D) The water content of NCMC/SA scaffolds; (E) SEM of the surface of NCMC/SA Scaffold; (F) SEM of the cross-section of NCMC/SA Scaffold. (Bar = 200 μm).

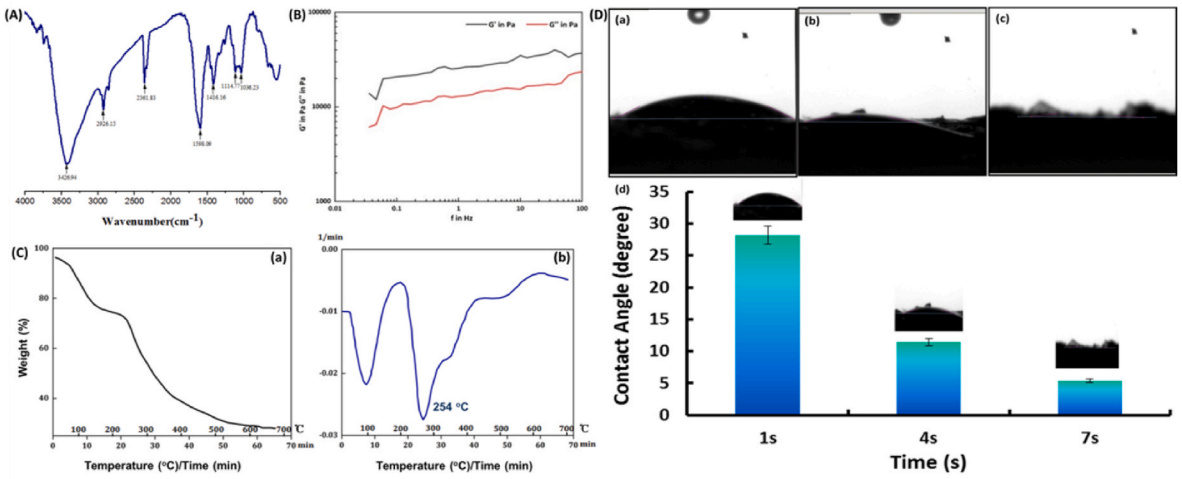

Fig. 2. The FTIR (A), rheological properties (B), TGA (C) and contact angles (D) results of NCMC/HA hydrogels. The (a), (b), and (c) images in figure (D) represented the images were recorded in 1, 4, and 7 s.

reported previously, the NCMC/SA hydrogel had satisfactory mechanical property. The TG test was considered as a sensitive method to estimate the content of the organic or inorganic matters in samples. Fig. 2 (C) showed the TG curves of NCMC/HA hydrogel from room temperature to 700 °C. The curves exhibited 11.4% weight loss at 100 °C, as a result of evaporating water content. An extremely high loss rate of 66.6% was observed at 240–320 °C, which corresponded to the thermal and oxidative decomposition of NCMC and HA. The literature had reported that the thermal decomposition of chitosan was between 217 and 300 °C, while that of sodium alginate was 200–248 °C [54–56]. As shown in Fig. 2 (D), the images were taken in 1, 4 and 7 s after the water dripped to the surface of the hydrogel, and the contact angels were 28.19°, 11.41° and 5.4°, respectively. The results showed that the water droplets could spread quickly on the surface of hydrogel and the NCMC/SA hydrogel had obvious hydrophilic properties.

The MTT assay was a received method to investigate the cytotoxicity of biomaterials and the results were shown in Fig. 3 (A). The cell viability of each concentration of the leaching liquor of the NCMC/SA scaffold was above 90% and there were also no cytotoxicity with the time going on, which demonstrated the good cytocompatibility of NCMC/SA scaffold. After cultured in NCMC/SA scaffold for 24 h and 48 h, the supernatant was taken and the lactate dehydrogenase (LDH) activity was measured using a LDH kit, as shown in Fig. 3 (B). At 24 h and 48 h, the relative proliferation rates of the NIH3T3 cells in the scaffold were 94.7% and 100.8%, respectively, indicating that the NCMC/SA scaffold was very helpful to the adherent growth of cells, which might be closely related to the NCMC component in the scaffold. Our previous studies had shown that the NCMC could promote the growth of fibroblast evidently. The NCMC/SA scaffold with NIH3T3 cells was treated with dehydration and carbon dioxide critical point drying, and the surface of the scaffold was observed by SEM, as shown in Fig. 3 (C). NIH3T3 cells grew in large numbers on the surface of the scaffold material, forming relatively complete cell lamellae, and showing extracellular matrix formed by the product secreted by the normal growth of

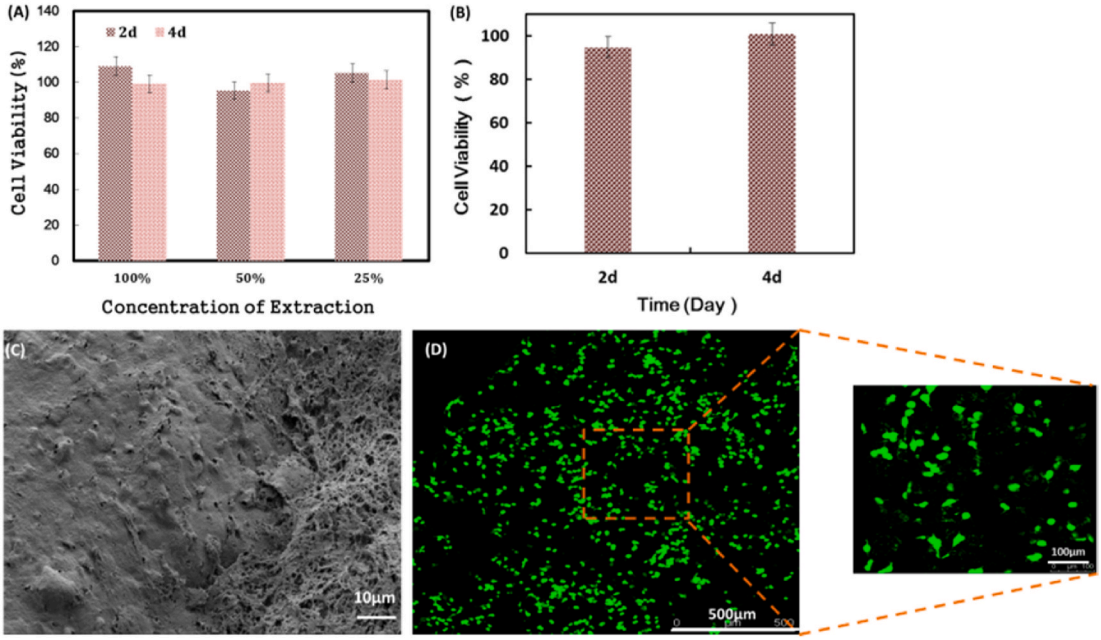

Fig. 3. (A) Cytocompatibility of Extraction of NCMC/SA Scaffold by MTT method; (B) Cytocompatibility of NCMC/SA scaffold with cells by LDH method; (C) SEM image of NCMC/SA scaffold with NIH3T3 cells at 48 h; (D) CLSM images of NCMC/SA scaffold with NIH3T3 cells at 48 h.

cells. The confocal laser images of the NIH3T3 nuclei in the scaffold after staining with Hoechst 33258 dye were shown in Fig. 3 (D). It could be seen that the large numbers of cells could grow inside the scaffold material, and they distributed evenly with good 3D cell growth effect.

The calculated maximum content of the Arg-CS/pDNA nanoparticles loaded in NCMC/SA scaffold was 21.9 μg/mg. The loading of plasmids by GAM could be realized in two ways [57–59]. The first approach was to integrate soluble plasmids with the scaffold by use of hydrogel swelling and water locking effect to load active factors. Another approach was to modify the surface of biological materials by chemical or physical methods to make the scaffold active and improve the bioactivity. For NS-GAM in this study, the genetic materials mainly entered into the hydrogel through the first way. When the Arg-CS/pDNA nanoparticles entered into the pores of the hydrogel, they could be further stably bound with the hydrogel through ionic effects, which interacted between Arg-CS and sodium alginate.

The release profile of the NS-GAM was presented in Fig. 4 (I). The release rate of the plasmids in pH 7.2 buffer was significantly faster than that in pH 5.0 and pH 1.45 buffers, indicating that the hydrogel had a sensitive release response in neutral environment, which was very important for its future application *in vivo*. The release rate of the nanoparticles in the early 10 days was much faster than that of the late 10 days. In the release of pH 7.2 buffer, the accumulated release rate was about 85% at day 10 and the accumulated release rate of the late 10 days was less than 5%. The total accumulated release rate for 20 days was 88.5%, which implied that most of the loaded nanoparticles could be released from the scaffold and the NS-GAM had a continuous release effect. As shown in Fig. 4 (I), the plasmids dissociated from the Arg-CS/pDNAs could be seen to have clear bands on the electrophoretic diagram, which proved that these plasmids released from the NS-GAM could still maintain their integrity. The SEM photographs (Fig. 4 (II)) showed that the pore size of the NS-GAM was 100 μm and nanoparticles could be observed on the wall of scaffold.

The *in vitro* gene transfection of NS-GAM was performed on NIH3T3 cells with pEGFP-C1 and pGL3-Luc as reporter genes and (pcDNA3.1(+)-mVEGF165 and pcDNA3.1(+)-TGF-β_1 as functional genes. Fig. 5 (A-E) displayed the typical fluorescence images of the transfected NIH3T3 cells. All the images showed green fluorescence and the transfection result of NS-GAM at day 9 exhibited the most notable green fluorescence. These results implied that the transfection efficiency of NS-GAM was closely related to the release time of Arg-CS/pDNA nanoparticles.

The pGL3-Luc gene transfection of the NS-GAM was evaluated with luciferase assay. As shown in Fig. 5 (F), the pGL3-Luc transfection efficiency at day 1 was only about 2×10^6 RLU/mg protein, while that at day 9 was more than 5.7×10^6 RLU/mg protein. The transfection activity at day 9 was 2.8-fold higher than that at day 1. These results were consistent with the pEGFP-C1 transfection results in Fig. 5 (A-E). The high activity of luciferase at day 9 also implied that the long time of 9 days release didn't destroy the activity of the protein.

The VEGF and TGF-β_1 gene transfection efficiencies were evaluated by Elisa Kits. As shown in Fig. 5 (G), both VEGF and TGF-β_1 had evident expression in NIH3T3 cells in in vitro transfection. The transfection efficiencies of both VEGF and TGF-β_1 were gradually enhanced with the release time and 3–4 fold higher at day 9 than those at day 1. The transfection efficiency increased much faster in the early 7 days and it became moderate in the later 2 days. These results implied that the functional genes such as VEGF and TGF-β_1 could be expressed in the NS-GAM system.

The surrounding tissues around implanted NS-GAM were taken out at day 3, 9, 15, 21 and 27 after implantation. As shown in Fig. 6 (I), mild acute inflammatory responses were observed both in control group and NS-GAM group at day 3. These phenomena were closely related to the foreign body reaction and surgical operation. Over time, the inflammatory response gradually decreased, and no tissue inflammatory response was observed at day 10 and day 20 after implantation. The results showed that NS-GAM had good histocompatibility *in vivo* and was suitable for subsequent wound repair studies. Fig. 6 (II) and (III) showed the *in vivo* degradation of NS-GAM. It could be seen from the trend line that the degradation rate of NS-GAM was fast in the first 3 days, and the degradation rate enters the plateau stage with little change after 20 days. At 27 days, NS-GAM still had nearly 40% proportion remaining. NCMC was the main degradation part of NS-GAM, which could be effectively degraded due to the presence of lysozyme *in vivo*. However, sodium alginate lacked the corresponding hydrolase, so the NS-GAM couldn't be completely degraded in the end.

The deep second-degree burn wounds treated by NS-GAM were studied comprehensively. Initially, we examined whether the NS-GAM promoted wound healing. And the results were showed in Fig. 7 (I). At 3 days, all the rats with burn wounds were carefully treated and there were no infection or contamination occurred. It was shown that wounds treated with normal saline were hemorrhagic and scab was present on the wound bed. After 12 days' treatment, the subcutaneous aspects in both groups changed normally and area of the wound became to a smaller size. The majority of the wound bed of NS-GAM group was nearly healed after 21 days. The majority of the subcutaneous aspects appeared nearly healed for NS-GAM group wounds at 21 days of post wounding.

As shown in Fig. 7 (II), by measuring the wound area at different intervals of time, the healing rate was calculated. In the first weak, both control group and NS-GAM group had low healing rate. At 10 days, there was obvious reduction in wound defect area for test whereas less reduction was observed in control group. In NS-GAM group, the first

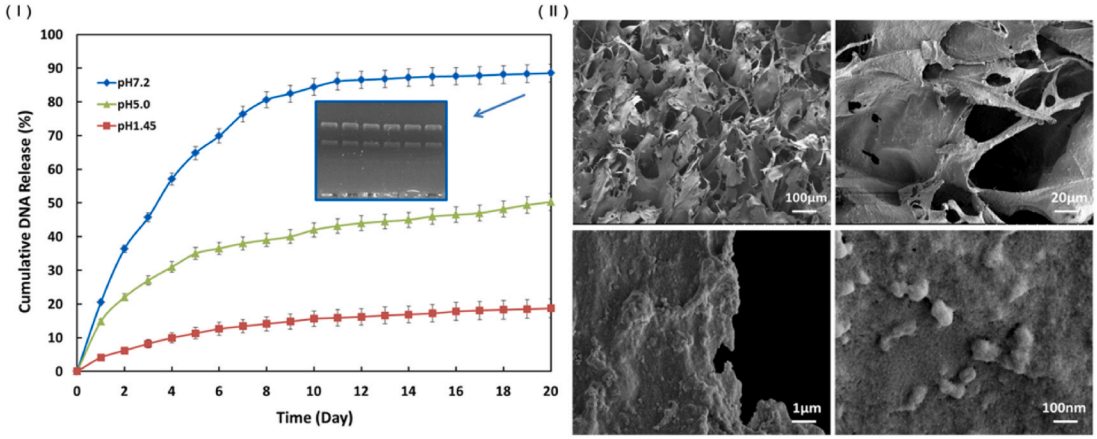

Fig. 4. *In vitro* release of pDNA from NS-GAM. (I) Cumulative amount of pDNA released *in vitro* from NS-GAM and the agarose gel electrophoresis of the plasmids; (II) SEM of the surface of NS-GAM.

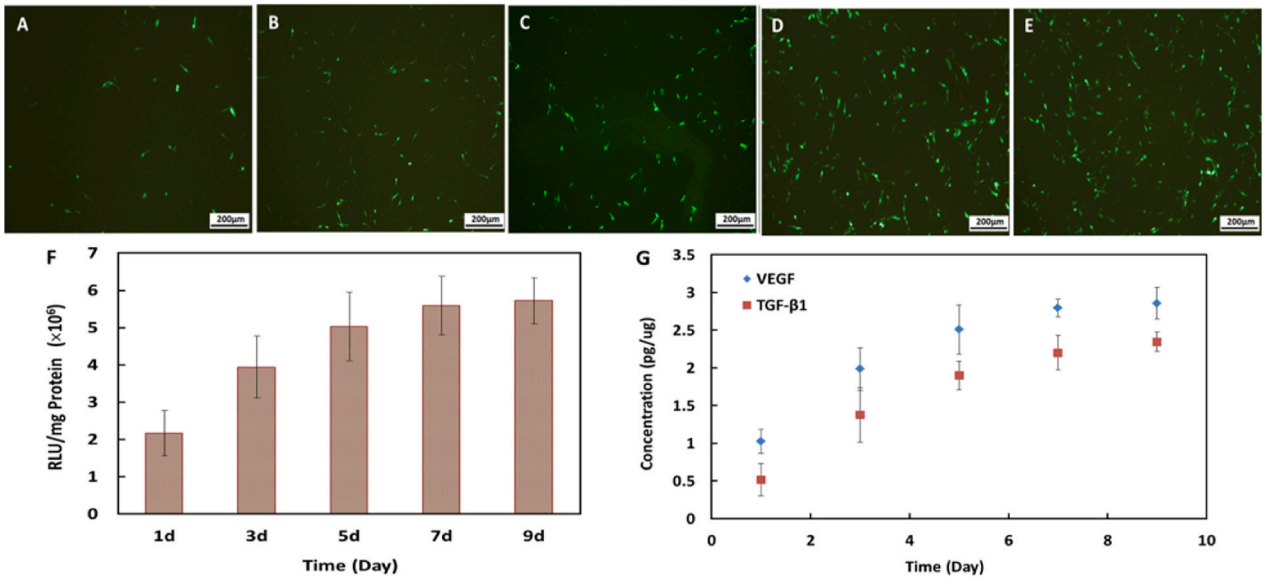

Fig. 5. Typical fluorescence images of GFP transfected by NS-GAM in different time. A: 1d, B: 3d, C: 5d, D: 7d, E: 9d; (F) Transfection efficiency of NS-GAM *in vitro*, the data were expressed as mean values (standard deviation)of six experiments; (G) Quantification of VEGF and TGF-β_1 by *in vitro* release from NS-GAM.

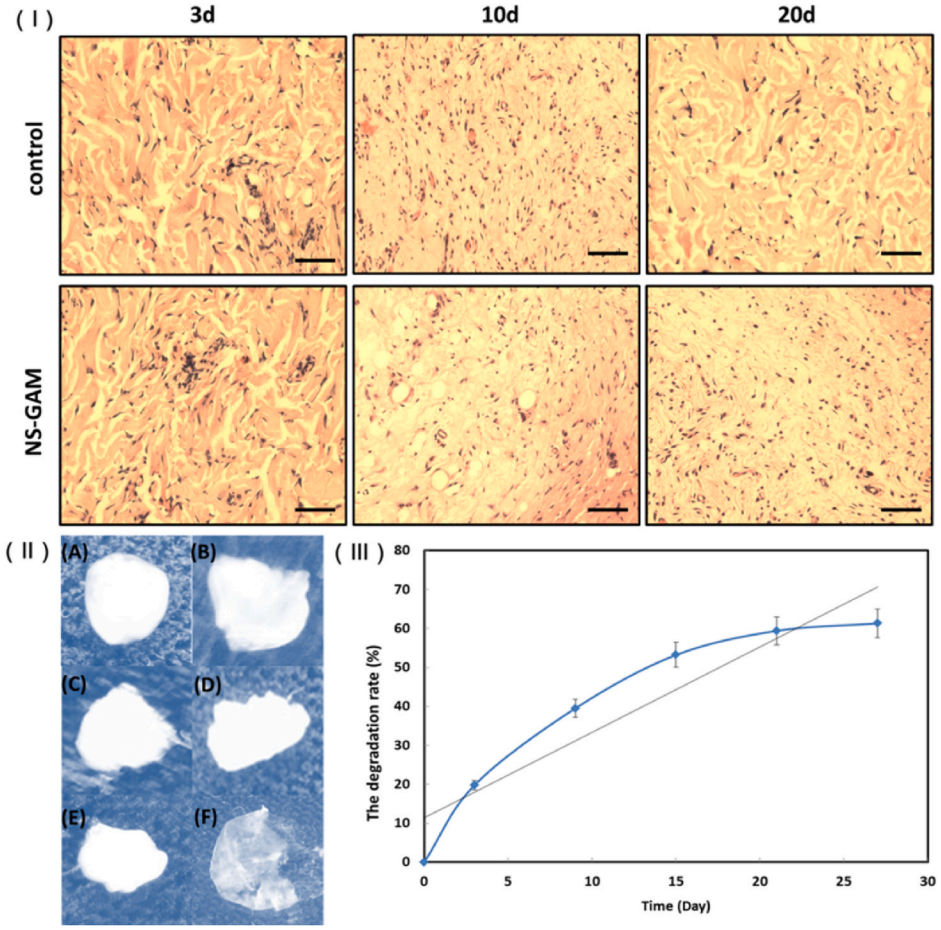

Fig. 6. *In vivo* histocompatibility and degradability of NS-GAM. (I) The histological photographs of HE staining (Bar = 100 μm); (II) Pictures of NS-GAM degradation at different times. A: 0d, B: 3d, C: 9d, D: 15d, E: 21d, F: 27d; (III) The degradation rate of NS-GAM *in vivo*.

complete closure was observed on day 16 and all wounds were healed by day 22. The first complete wound closure in control group was observed on days 22 and all wounds were healed by day 30, respectively. At 22 days, healing was complete for wounds treated with NS-GAM leading to about 100% fill in wound defect. This was only about 78.9% in control group. The difference was statistically significant from day 14 between

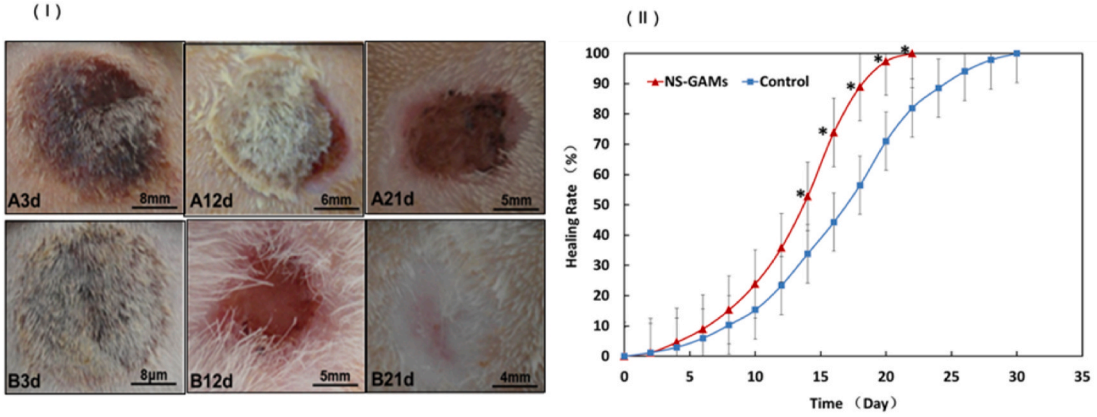

Fig. 7. Gross examination and healing rate. (I) Observation of the deep second degree burn wounds. A: Control group; B: NS-GAM group. (II) The calculated wound size reduction. *Significant difference from control at the same time ($p < 0.05$).

control group and NS-GAM group ($p < 0.05$).

The rats were sacrificed on day 3, 12, and 21, the healing procedure was observed via the pathological section stained by HE staining. The inflammatory response was one of the most important factors for early-stage wound healing and the inflammatory responses in the two groups were compared. As show in Fig. 8 (I), severe inflammation reaction and evident necroses occurred in the superficial layers of the wounds in control group on day 3. Both the control group and the NS-GAM group showed acute inflammatory response at 3d, and the number of the inflammatory cells in control group was more than 1000. It was also shown that the dermis of the burn wound was damaged in different degrees. The area sizes of the wounds were obviously reduced and inflammation became mild on day 12. The granulation tissue was accelerated in both groups and the NS-GAM group had the smaller amount of granulation tissue. The occurrence of new epithelialization was a typical characteristic in the superficial layers of the wounds treated with NS-GAM scaffold. It was reported that the formation of granulation tissue was essential for the permanent closure of wounds because it filled the defect and prepared the way for epithelialization [60]. However, the occurrence of hyperplasia phenomenon in the epithelial lining was the typical characteristic in control group, which might due to the inflammatory hyperplasia caused by sever inflammatory reaction [61]. On day 21, the defect area disappeared and it was covered with new and integral epithelium in the NS-GAM group, the dermis showed favorable recovery in its depth and elasticity. Little inflammation was present in the wounds of NS-GAM and control group, and the numbers of the inflammatory cells were less than 100. The dermis of control group showed poor recovery, in which the epithelialization was uncompleted on the surface of the wounds.

Collagen was an important index in the evaluation of the wound healing, which was the most abundant protein in the dermis and closely related to the strength, structure and elasticity in wound healing [62]. The collagen remodeling and maturation was stained and highlighted by Masson's Trichrome staining. As shown in Fig. 8 (II), the collagen in

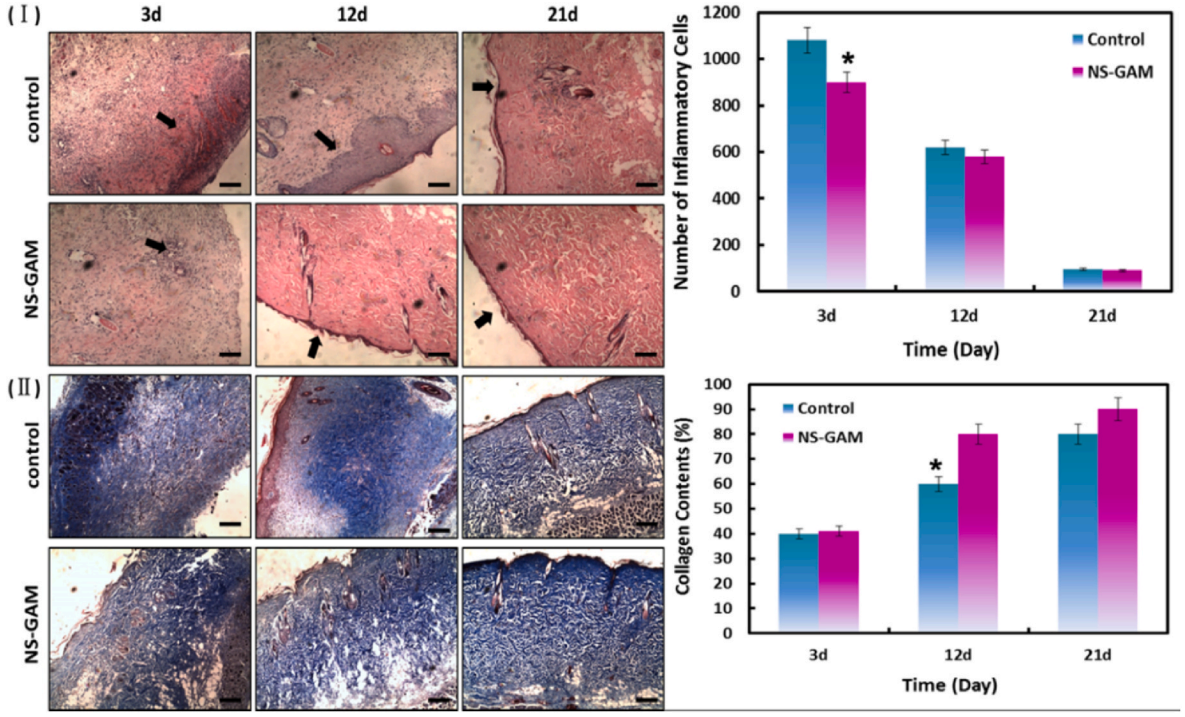

Fig. 8. Histological examination of deep-second degree burn wound. (I) The histological photographs of HE staining; (II) The collagen content of control group and NCMC group at different times. A: Control group; B: NS-GAM group.

both groups of NS-GAM and control were destroyed and cross-linked after burn wounding, which remained only less than 40%. At each time point, the NS-GAM treated wounds had more mature collagen development compared to the wounds in control group. New formed collagen could be seen in the dermis on day 12 and the mature collagen with the proportion of more than 90% was observed in the dermis in NS-GAM group on day 21. The collagen fibers in NS-GAM group were abundant and regular, while those in the control group were still somewhat discrete and irregular. This result implied that the healing effect of NS-GAM was much better than that of control.

The amounts of VEGF and TGF-β_1 were determined on the day 1, 3, 5, 7, 9, 12, and 15 after the treatment of ELISA Kits. VEGF was the main factor to create new blood vessels after injury and encouraged new vessels to form circulation to bypass blocked vessels [63]. As shown in Fig. 9 (I), the amount of TGF-β_1 at the wound area in NS-GAM group was higher than that of control, the significant differences appeared on day 3 and 5. TGF-β_1 was an important growth factor for wound repair [64], its functions included promotion of fibroblasts proliferation, increasing deposition of connective tissue, transformation of fibroblasts into myofibroblasts and wound contraction. TGF-β_1 could facilitate the synthesis of collagen I/III and elastin in fibroblasts, repress matrix metalloproteinases (MMPs) activity, enhance fibronectin expression, decrease collagen fibers degradation and promote the exudation of ECM [65]. It was reported that the increase of TGF-β_1 was favorable for wound contraction and repair. The amounts of VEGF at the wound area in NS-GAM treated samples were higher in each time points and showed significant differences on day 5, 7 and 9 compared to the control group (Fig. 9 (II)), which was attributed to the release of VEGF-gene from the NS-GAM. The results implied that the revascularization of NS-GAM group was much better than that of control group. As can be seen from the immunohistochemical results in Fig. 9 (III), the staining areas of VEGF and TGF-β_1 in NS-GAM group were significantly more than those in the control group, with higher expression levels. These results were consistent with the quantification analysis. According to the literature reported [66–68], the dose of TGF-β_1 and VEGF was up to 10^{-1}-10^4 pg/mL in cell experiment and 2–5 ng/cm^2 in local injection *in vivo*. By detecting the expression levels of proteins, it could be seen that the expression levels were within the safe dose even the plasmids were used according to the maximum loading amount. In the experiment of the scalded rats, there was no scar or hyperplasia observed in the NS-GAM group, indicating that the concentration of the plasmid was within the safe dose.

As the blood vessels of the skin were in the dermis, the blood flow velocity of the wounds area was an important index to reflect the dermis recovery in deep-second degree burn wounds. As shown in Fig. 10, the normal blood flow velocity was about 120 mm^3/s. The blood flow velocity decreased to about 60 mm^3/s after 1d of the burn wounds, it was the half of the normal blood flow velocity. The blood flow velocity increased quickly during 5–12 days after burn wounds and the blood flow velocity of NS-GAM group increased much faster than that of control group. The different recovery of blood flow velocity in the two groups was due to the gene activity of VEGF released from NS-GAM scaffold. The neoformative blood vessels could do favorable effort on the healing of the burn wounds. CD34 was a transmembrane

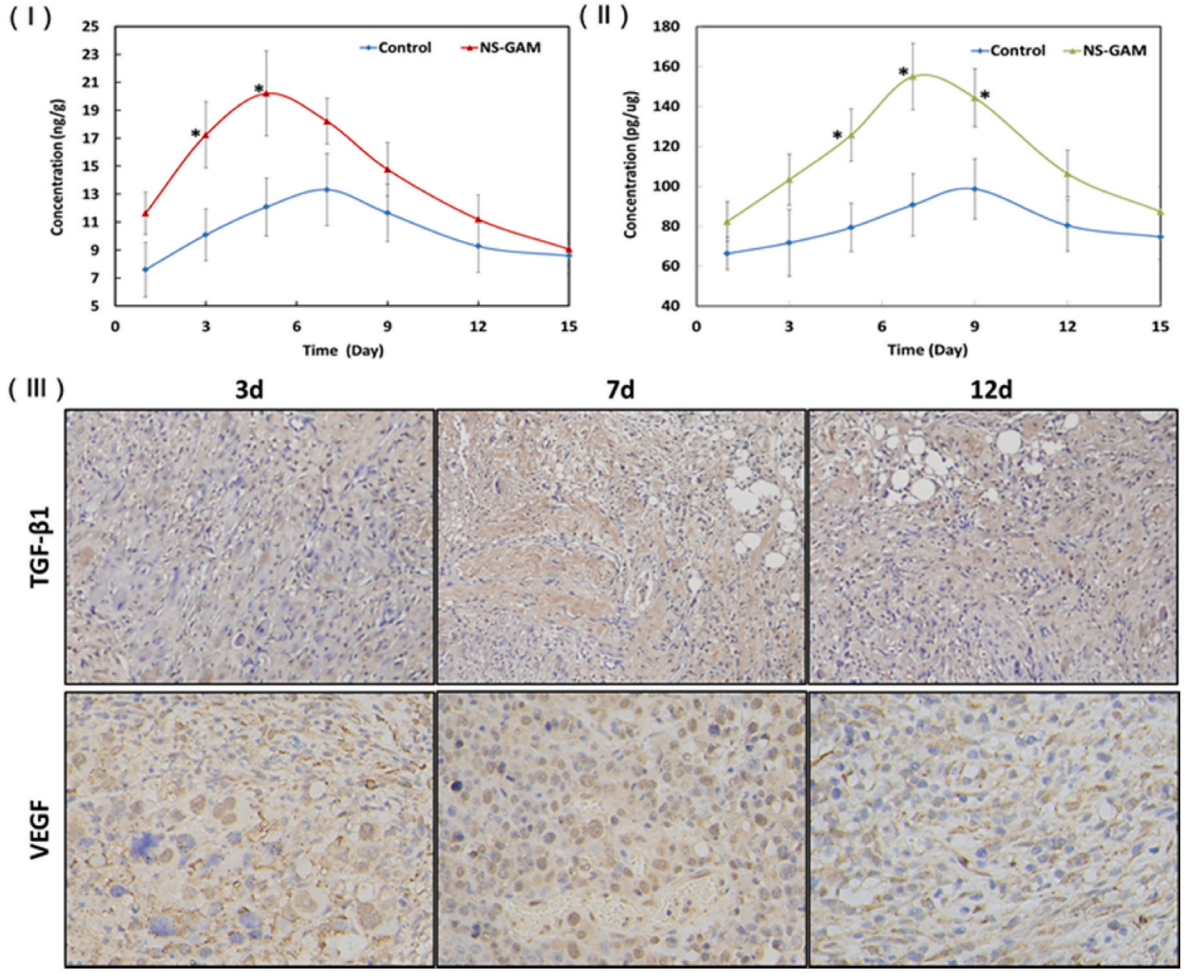

Fig. 9. Expression of VEGF and TGF-β_1 *in vivo*. (I) Quantification of VEGF of the wound area at different time, *: Significant difference from control at the same time ($p < 0.05$); (II) The histological paragraph on TGF-β_1 and VEGF immunohistochemisty; (III) Quantification of TGF-β_1 of the wound area at different time.

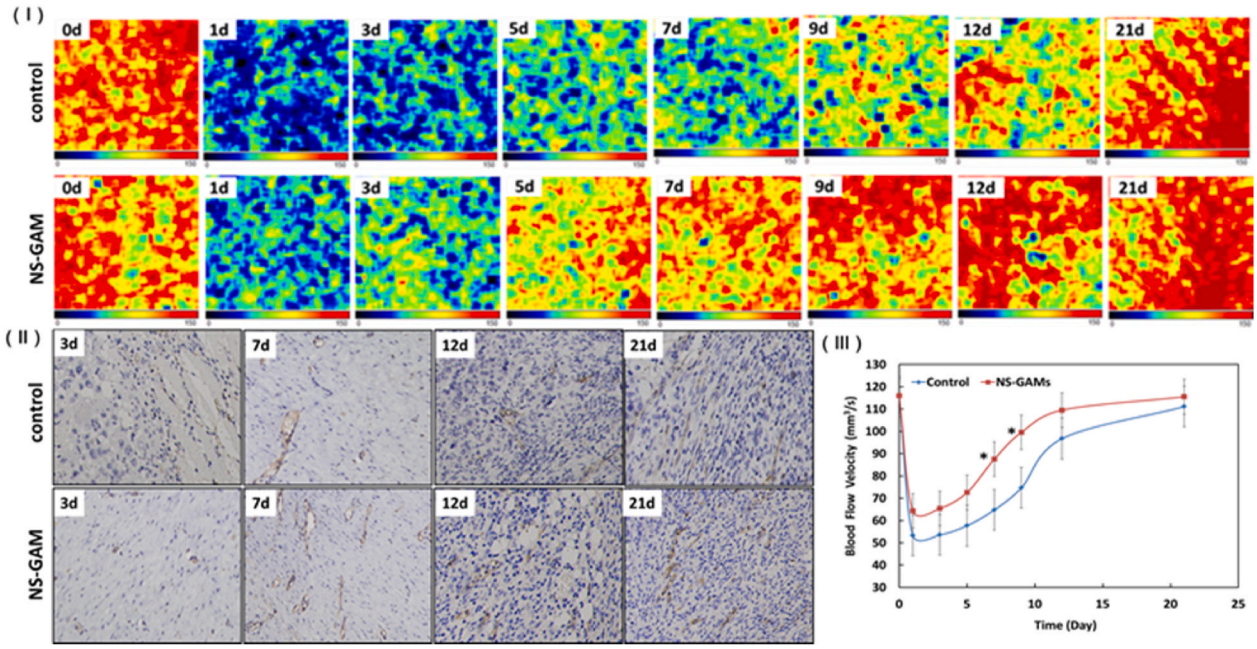

Fig. 10. Results of blood flow velocity of the burn wound. (I) Images of bloodflow velocity of the wound area at different time; (II) The histological paragraph on CD34 immunohistochemisty; (III) Quantification of blood flow velocity of the wound area at different time. *: Significant difference from control at the same time ($p < 0.05$).

glycoprotein expressed on the surface of normal endothelial cells and it was often used as a marker of vascular endothelial cells in neovascularization studies. The immunohistochemical results showed that the expression level of CD34 was higher in NS-GAM group compared with the control group, which was consistent with the results of blood flow velocity, suggesting that there were more abundant neovascularization in NS-GAM group.

4. Conclusion

In this study, a novel NS-GAM composed of *N*-carboxymethyl chitosan/sodium alginate hybrid scaffold and therapeutic genes/vector complex nanoparticles was prepared, the function of NS-GAM on the healing and regeneration of deep second degree burn wound was evaluated. The results demonstrated that the NS-GAM exhibited excellent gene delivery capability with successful GFP and luciferase expression *in vitro* and high VEGF and TGF-β_1 protein expression both *in vitro* and *in vivo*. The healing of deep second degree burn wound was accelerated evidently by the treatment of NS-GAM, the healing time was about 22 days after burn injury. The pathological examination results showed that the NS-GAM treated wounds generated milder inflammation reaction and better epithelialization. Moreover, the mature collagen was abundant and ordered in NS-GAM group, the wounds treated with NS-GAM exhibited faster recovery of blood flow velocity. The NS-GAM was expected to be used as a promising wound healing material to promote the repair of deep second-degree burn wound and the idea of GAM gave an important strategy for skin regeneration application in future.

CRediT authorship contribution statement

Litong Wang: Conceptualization, Methodology, Writing – original draft. **Le Sun:** Conceptualization, Writing – original draft. **Zhiyang Gu:** Investigation. **Wenya Li:** Formal analysis. **Lili Guo:** Investigation. **Saibo Ma:** Validation. **Lan Guo:** Validation. **Wangwang Zhang:** Formal analysis. **Baoqin Han:** Resources. **Jing Chang:** Supervision, Project administration, Writing – review & editing.

Declaration of competing interest

The authors declare no conflict of interest.

Acknowledgement

The authors wish to thank National Natural Science Foundation of China (No. 51773188), Key Project of Natural Science Foundation of Shandong Province (No. ZR2020KE016), The National Key Research and Development Program of China (No. 2018YFC1105602, 2018YFD0900601).

Appendix A. Supplementary data

Supplementary data to this article can be found online at https://doi.org/10.1016/j.bioactmat.2021.12.012.

References

[1] A.V. Nguyen, A.M. Soulika, The dynamics of the skin's immune system, Int. J. Mol. Sci. 20 (8) (2019) 1811–1864, https://doi.org/10.3390/ijms20081811.
[2] S. Eyerich, K. Eyerich, C. Traidl-Hoffmann, T. Biedermann, Cutaneous barriers and skin immunity: differentiating a connected network, Trends Immunol. 39 (4) (2018) 315–327, https://doi.org/10.1016/j.it.2018.02.004.
[3] S. Takahashi, D. Hashimoto, E. Hayase, R. Ogasawara, H. Ohigashi, T. Ara, E. Yokoyama, K. Ebata, S. Matsuoka, G.R. Hill, J. Sugita, M. Onozawa, T. Teshima, Ruxolitinib protects skin stem cells and maintains skin homeostasis in murine graft-versus-host disease, Blood 131 (18) (2018) 2074–2085, https://doi.org/10.1182/blood-2017-06-792614.
[4] Y. Wang, J. Beekman, J. Hew, S. Jackson, A.C. Issler-Fisher, R. Parungao, S. S. Lajevardi, Z. Li, P. Maitz, Burn injury: challenges and advances in burn wound healing, infection, pain and scarring, Adv. Drug Deliv. Rev. 123 (2018) 3–17, https://doi.org/10.1016/j.addr.2017.09.018.
[5] J.L. Medina, E.A. Sebastian, A.B. Fourcaudot, R. Dorati, K.P. Leung, Pirfenidone ointment modulates the burn wound bed in C57BL/6 mice by suppressing inflammatory responses, Inflammation 42 (1) (2019) 45–53, https://doi.org/10.1007/s10753-018-0871-y.
[6] Z. Ghlissi, R. Kallel, F. Krichen, A. Hakim, K. Zeghal, T. Boudawara, A. Bougatef, Z. Sahnoun, Polysaccharide from pimpinella anisum seeds: structural characterization, anti-inflammatory and laser burn wound healing in mice, Int. J. Biol. Macromol. 156 (2020) 1530–1538, https://doi.org/10.1016/j.ijbiomac.2019.11.201.

[7] J.C. Brazil, M. Quiros, A. Nusrat, C.A. Parkos, Innate immune cell-epithelial crosstalk during wound repair, J. Clin. Invest. 129 (8) (2019) 2983–2993, https://doi.org/10.1172/JCI124618.
[8] J. Zhong, H. Wang, K. Yang, H. Wang, C. Duan, N. Ni, L. An, Y. Luo, P. Zhao, Y. Gou, S. Sheng, D. Shi, C. Chen, W. Wagstaff, H.S. Bryce, R.C. Haydon, J. Fan, Reversibly immortalized keratinocytes (iKera) facilitate re-epithelization and skin wound healing: potential applications in cell-based skin tissue engineering, Bioact. Mater. 22 (2021) 2451–2469, https://doi.org/10.1016/j.bioactmat.2021.07.022.
[9] A. Andrade, P. Brassolatti, G.F. Luna, J.R. Parisi, Â.M. Oliveira Leal, M. Frade, N. A. Parizotto, Effect of photobiomodulation associated with cell therapy in the process of cutaneous regeneration in third degree burns in rats, J. Tissue Eng. Reg. Med. 14 (5) (2020) 673–683, https://doi.org/10.1002/term.3028.
[10] W. Liu, M. Wang, W. Cheng, W. Niu, M. Chen, M. Luo, C. Xie, T. Leng, L. Zhang, B. Lei, Bioactive antiinflammatory antibacterial hemostatic citrate-based dressing with macrophage polarization regulation for accelerating wound healing and hair follicle neogenesis, Bioact. Mater. 3 (6) (2021) 721–728, https://doi.org/10.1016/j.bioactmat.2020.09.008.
[11] M.S. Annapoorna, D.R. Biswas, R. Jayakumar, Chitosan based metallic nanocomposite scaffolds as antimicrobialwound dressings, Bioact. Mater. 3 (3) (2018) 267–277, https://doi.org/10.1016/j.bioactmat.2017.11.003.
[12] H. Zhang, M. Peng, S. Li, Y. Zhang, Y. Gao, W.H. Lee, Carboxymethyl chitosan nanoparticles loaded with bioactive peptide OH-CATH30 benefit nonscar wound healing, Int. J. Nanomed. 13 (2018) 5771–5786, https://doi.org/10.2147/IJN.S156206.
[13] Z. Zhang, W. Zhang, Y. Li, Z. Liu, L. Yang, H. Ma, E. Zhang, C. Wang, Z. Wu, F. Huang, J. Guo, Design of a biofluid-absorbing bioactive sandwich-structured Zn–Si bioceramic composite wound dressing for hair follicle regeneration and skin burn wound healing, Bioact. Mater. 7 (6) (2020) 1910–1920, https://doi.org/10.1016/J.bioactmat.2020.12.006.
[14] Y. Wu, G. Wu, H. Huang, S. Kuo, Liposome-encapsulated farnesol accelerated tissue repair in third-degree burns on a rat model, Burns 45 (5) (2019) 1139–1151, https://doi.org/10.1016/j.burns.2019.01.010.
[15] C.A. Ocon, S.A. Santos, J.R. Caires, M. Oliveira, A.J. Serra, E.C. Leal-Junior, P. Carvalho, Effects and parameters of the photobiomodulation in experimental models of third-degree burn: systematic review, Las, Med. Sci. 34 (3) (2019) 637–648, https://doi.org/10.1007/s10103-018-2633-3.
[16] D.M. Burmeister, R. Stone, N. Wrice, A. Laborde, S.C. Becerra, S. Natesan, R. J. Christy, Delivery of allogeneic adipose stem cells in polyethylene glycol-fibrin hydrogels as an adjunct to meshed autografts after sharp debridement of deep partial thickness burns, J. Tissue Eng. Reg. Med. 7 (4) (2018) 360–372, https://doi.org/10.1002/sctm.17-0160.
[17] F. Tang, J. Li, W. Xie, Y. Mo, L. Yang, F. Zhao, X. Fu, X. Chen, Bioactive glass promotes the barrier functional behaviors of keratinocytes and improves the Re-epithelialization in wound healing in diabetic rats, Bioact. Mater. 10 (6) (2021) 3496–3506, https://doi.org/10.1016/j.bioactmat.2021.02.041.
[18] T. Mehrabi, A.S. Mesgar, Z. Mohammadi, Bioactive classes: a promising therapeutic ion release strategy for enhancing wound healing, ACS Bio. Mater. Sci. Eng. 6 (10) (2020) 5399–5430, https://doi.org/10.1021/acsbiomaterials.0c00528.
[19] F. Yi, F. Guo, Y. Li, D. Wang, P. Huang, S. Fu, Polyacrylamide hydrogel composite E-skin fully mimicking human skin, ACS Appl. Mater. Interfaces 27 (13) (2021) 32084–32093, https://doi.org/10.1021/acsami.1c05661.
[20] J. Li, F. Yu, G. Chen, J. Liu, X.L. Li, B. Cheng, X.M. Mo, C. Chen, J.F. Pan, Moist-retaining, self-recoverable, bioadhesive, and transparent in situ forming hydrogels to accelerate wound healing, ACS Appl. Mater. Interfaces 12 (2) (2020) 2023–2038, https://doi.org/10.1021/acsami.9b17180.
[21] A.R. Abbasi, M. Sohail, M.U. Minhas, T. Khaliq, M. Kousar, S. Khan, Z. Hussain, A. Munir, Bioinspired sodium alginate based thermosensitive hydrogel membranes for accelerated wound healing, Int. J. Biol. Macromol. 155 (2020) 751–765, https://doi.org/10.1016/j.ijbiomac.2020.03.248.
[22] Y. Liang, J. He, B. Guo, Functional hydrogels as wound dressing to enhance wound healing, ACS Nano 8 (15) (2021) 12687–12722, https://doi.org/10.1021/acsnano.1c04206.
[23] Y. li, R. Fu, Z. Duan, C. Zhu, D. Fan, Construction of multifunctional hydrogel based on the tannic acid-metal coating decorated MoS_2 dual nanozyme for bacteria-infected wound healing, Bioact. Mater. 22 (7) (2021) 2452–2466, https://doi.org/10.1016/j.bioactmat.2021.07.023.
[24] Y. Yang, Y. Liang, J. Chen, X. Duan, B. Guo, Mussel-inspired adhesive antioxidant antibacterial hemostatic composite hydrogel wound dressing via photo-polymerization for infected skin wound healing, Bioact. Mater. 8 (2021) 341–354, https://doi.org/10.1016/j.bioactmat.2021.06.014.
[25] P. Rao, T.L. Sun, L. Chen, R. Takahashi, G. Shinohara, H. Guo, D.R. King, T. Kurokawa, J.P. Gong, Tough hydrogels with fast, strong, and reversible underwater adhesion based on a multiscale design, Adv. Mater. 30 (32) (2018), e1801884, https://doi.org/10.1002/adma.201801884.
[26] L. Kong, Z. Wu, H. Zhao, H. Cui, J. Shen, J. Chang, H. Li, Y. He, Bioactive injectable hydrogels containing desferrioxamine and bioglass for diabetic wound healing, ACS Appl. Mater. Interfaces 10 (36) (2018) 30103–30114, https://doi.org/10.1021/acsami.8b09191.
[27] A. Wubneh, E.K. Tsekoura, C. Ayranci, H. Uludağ, Current state of fabrication technologies and materials for bone tissue engineering, Acta Biomater. 80 (2021) 1–30, https://doi.org/10.1016/j.actbio.2018.09.031.
[28] Y. Wang, R.K. Kankala, C. Ou, A. Chen, Z. Yang, Advances in hydrogel-based vascularized tissues for tissue repair and drug screening, Bioact. Mater. 5 (7) (2021) 2452–2475, https://doi.org/10.1016/j.bioactmat.2021.07.005.
[29] W. Yin, E. Smiley, J. Germiller, R.P. Mecham, J.B. Florer, R.J. Wenstrup, J. Bonadio, Isolation of a novel latent transforming growth factor-beta binding protein gene (LTBP-3), J. Bio. Chem. 270 (17) (1995) 10147–10160, https://doi.org/10.1074/jbc.270.17.10147.
[30] D. Lou, Y. Luo, Q. Pang, W. Tan, L. Ma, Gene-activated dermal equivalents to accelerate healing of diabetic chronic wounds by regulating inflammation and promoting angiogenesis, Bioact. Mater. 3 (5) (2020) 667–679, https://doi.org/10.1016/j.bioactmat.2020.04.018.
[31] R. Shido, Y. Sumita, M. Hara, M. Iwatake, S. Narahara, M. Umebayashi, K.I. Miura, Y. Kodama, I. Asahina, Gene-activated matrix harboring a miR20a-expressing plasmid promotes rat cranial bone augmentation, Regen. Biomater. 8 (2) (2021) 1–9, https://doi.org/10.1093/rb/rbaa060.
[32] Y. Zha, T. Lin, Y. Li, X. Zhang, Z. Wang, Z. Li, Y. Ye, B. Wang, S. Zhang, J. Wang, Exosome-mimetics as an engineered gene-activated matrix induces in-situ vascularized osteogenesis, Biomaterials 247 (2020) 119985, https://doi.org/10.1016/j.biomaterials.2020.119985.
[33] L. Yin, X. Zhao, S. Ji, C. He, G. Wang, C. Tang, S. Gu, C. Yin, The use of gene activated matrix to mediate effective SMAD2 gene silencing against hypertrophic scar, Biomaterials 35 (8) (2014) 2488–2498, https://doi.org/10.1016/j.biomaterials.2013.12.015.
[34] Z. Zheng, M. Li, P. Shi, Y. Gao, J. Ma, Y. Li, L. Huang, Z. Yang, L. Yang, Polydopamine-modified collagen sponge scaffold as a novel dermal regeneration template with sustained release of platelet-rich plasma to accelerate skin repair: a one-step strategy, Bioact. Mater. 8 (6) (2021) 2613–2628, https://doi.org/10.1016/j.bioactmat.2021.01.037.
[35] J. Yang, M. Shen, Y. Luo, T. Wu, H. Wen, J. Xie, Construction and characterization of Mesona chinensis polysaccharide-chitosan hydrogels, role of chitosan deacetylation degree, Carbohydr. Polym. 257 (2021) 117608, https://doi.org/10.1016/j.carbpol.2020.117608.
[36] T. Sun, B. Zhan, W. Zhang, D. Qin, G. Xia, H. Zhang, M. Peng, S.A. Li, Y. Zhang, Y. Gao, W.H. Lee, Carboxymethyl chitosan nanoparticles loaded with bioactive peptide OH-CATH30 benefit nonscar wound healing, Int. J. Nanomed. 13 (2018) 5771–5786, https://doi.org/10.2147/IJN.S156206.
[37] B. Mai, M. Jia, S. Liu, Z. Sheng, M. Li, Y. Gao, X. Wang, Q. Liu, P. Wang, Hydrogel-based DVDMS/bFGF nanohybrids for antibacterial phototherapy with multiple damaging sites and accelerated wound healing, ACS Appl. Mater. Interfaces 9 (12) (2020) 10156–10169, https://doi.org/10.1021/acsami.0c00298.
[38] H. Xue, L. Hu, Y. Xiong, X. Zhu, C. Wei, F. Cao, W. Zhou, Y. Sun, Y. Endo, M. Liu, Y. Liu, J. Liu, A. Abududilibaier, L. Chen, C. Yan, B. Mi, G. Liu, Quaternized chitosan-matrigel-polyacrylamide hydrogels as wound dressing for wound repair and regeneration, Carbohydr. Polym. 226 (2019) 115302, https://doi.org/10.1016/j.carbpol.2019.115302.
[39] S. Sapru, S. Das, M. Mandal, A.K. Ghosh, S.C. Kundu, Sericin-chitosan-glycosaminoglycans hydrogels incorporated with growth factors for in vitro and in vivo skin repair, Carbohydr. Polym. 258 (2021) 117717, https://doi.org/10.1016/j.carbpol.2021.117717.
[40] J. Chang, W. Liu, B. Han, S. Peng, B. He, Z. Gu, Repair and healing mechanism investigation of N-Carboxymethyl chitosan on deep second-degree burn wound, Wound Repair Regen. 21 (1) (2013) 113–121, https://doi.org/10.1111/j.1524-475X.2012.00859.x.
[41] D. Remias, C. Nicoletti, K. Krennhuber, B. Möderndorfer, L. Nedbalová, L. Procházková, Growth, fatty, and amino acid profiles of the soil alga Vischeria sp. E71.10 (Eustigmatophyceae) under different cultivation conditions, Folia Microbiol. 65 (6) (2020) 1017–1023, https://doi.org/10.1007/s12223-020-00810-8.
[42] J. Mesquita, J.P. Castro-de-Sousa, S. Vaz-Pereira, A. Neves, L.A. Passarinha, C. T. Tomaz, Vascular endothelial growth factors and placenta growth factor in retinal vasculopathies: current research and future perspectives, Cytokine Growth Factor Rev. 39 (2018) 102–115, https://doi.org/10.1016/j.cytogfr.2017.11.005.
[43] J.G. Yang, L.L. Wang, D.C. Ma, Effects of vascular endothelial growth factors and their receptors on megakaryocytes and platelets and related diseases, Br. J. Haematol. 180 (3) (2018) 321–334, https://doi.org/10.1111/bjh.15000.
[44] X. Han, M. Sun, B. Chen, Q. Saiding, J. Zhang, H. Song, L. Deng, P. Wang, W. Gong, W. Cui, Lotus seedpod-inspired internal vascularized 3D printed scaffold for bone tissue repair, Bioact. Mater. 6 (6) (2021) 1639–1652, https://doi.org/10.1016/j.bioactmat.2020.11.019.
[45] S. Liarte, Á. Bernabé-García, F.J. Nicolás, Role of TGF-β in skin chronic wounds: a keratinocyte perspective, Cells 9 (2) (2020) 306–323, https://doi.org/10.3390/cells9020306.
[46] T. Paramasivam, S.K. Maiti, S. Palakkara, D. Mohan, H.V. Manjunthaachar, K. Karthik, N. Kumar, Effect of PDGF-B gene-activated acellular matrix and mesenchymal stem cell transplantation on full thickness skin burn wound in rat model, J. Tissue Eng. Regen. Med. 18 (2) (2021) 235–251, https://doi.org/10.1007/s13770-020-00302-3.
[47] C. Li, G. Zhen, Y. Chai, L. Xie, J.L. Crane, E. Farber, C.R. Farber, X. Luo, P. Gao, X. Cao, M. Wan, RhoA determines lineage fate of mesenchymal stem cells by modulating CTGF-VEGF complex in extracellular matrix, Nat. Nanotechnol. 7 (2016) 11455, https://doi.org/10.1038/ncomms11455.
[48] J. Chang, X. Xu, H. Li, Y. Jian, G. Wang, B. He, Z. Gu, Components simulation of viral envelope via amino acid modified chitosans for efficient nucleic acid delivery: in vitro and in vivo study, Adv. Funct. Mater. 23 (21) (2013) 2691–2699, https://doi.org/10.1002/adfm.201202503.
[49] T. Mehrabi, A.S. Mesgar, Z. Mohammadi, Bioactive glasses: a promising therapeutic ion release strategy for enhancing wound healing, ACS Biomater. Sci. Eng. 6 (10) (2020) 5399–5430, https://doi.org/10.1021/acsbiomaterials.0c00528.
[50] S. Kondaveeti, P. Bueno, A.M. Carmona-Ribeiro, F. Esposito, N. Lincopan, M. R. Sierakowski, D. Petri, Microbicidal gentamicin-alginate hydrogels, Carbohydr. Polym. 186 (2018) 159–167, https://doi.org/10.1016/j.carbpol.2018.01.044.

[51] R.R. Palem, K. Madhusudana Rao, T.J. Kang, Self-healable and dual-functional guar gum-grafted-polyacrylamidoglycolic acid-based hydrogels with nano-silver for wound dressings, Carbohydr. Polym. 223 (2019) 115074, https://doi.org/10.1016/j.carbpol.2019.115074.

[52] L. Meng, C. Shao, C. Cui, F. Xu, J. Lei, J. Yang, Autonomous self-healing silk fibroin injectable hydrogels formed via surfactant-free hydrophobic association, ACS Appl. Mater. Interfaces 12 (1) (2020) 1628–1639, https://doi.org/10.1021/acsami.9b19415.

[53] Z. Zheng, M. Li, P. Shi, Y. Gao, J. Ma, Y. Li, L. Huang, Z. Yang, L. Yang, Polydopamine-modified collagen sponge scaffold as a novel dermal regeneration template with sustained release of platelet-rich plasma to accelerate skin repair: a one-step strategy, Bioact. Mater. 8 (6) (2021) 2613–2628, https://doi.org/10.1016/j.bioactmat.2021.01.037.

[54] X. Sun, C. Liu, A.M. Omer, L.Y. Yang, X.K. Ouyang, Dual-layered pH-sensitive alginate/chitosan/kappa-carrageenan microbeads for colon-targeted release of 5-fluorouracil, Int. J. Biol. Macromol. 132 (2019) 487–494, https://doi.org/10.1016/j.ijbiomac.2019.03.225.

[55] W. Zhang, C. Shu, Q. Chen, J. Cao, W. Jiang, The multi-layer film system improved the release and retention properties of cinnamon essential oil and its application as coating in inhibition to penicillium expansion of apple fruit, Food Chem. 299 (2019) 125109, https://doi.org/10.1016/j.foodchem.2019.125109.

[56] M. Rizwan, K.M. Zia, M.A. Javaid, M. Zuber, W. Aftab, S. Rehman, Synthesis and molecular characterization of chitosan/alginate blends based polyurethanes biocomposites, Int. J. Biol. Macromol. 180 (2021) 324–331, https://doi.org/10.1016/j.ijbiomac.2021.03.064.

[57] L. Chen, Z. Li, Y. Zheng, F. Zhou, J. Zhao, Q. Zhai, Z. Zhang, T. Liu, Y. Chen, S. Qin, 3D-printed dermis-specific extracellular matrix mitigates scar contraction via inducing early angiogenesis and macrophage M2 polarization, Bioact. Mater. 9 (2021), https://doi.org/10.1016/j.bioactmat.2021.09.008.

[58] Y. Luo, L. Fan, C. Liu, H. Wen, S. Wang, P. Guan, D. Chen, C. Ning, L. Zhou, G. Tan, An injectable, self-healing, electroconductive extracellular matrix-based hydrogel for enhancing tissue repair after traumatic spinal cord injury, Bioact. Mater. 7 (2021) 98–111, https://doi.org/10.1016/j.bioactmat.2021.05.039.

[59] T.M. Marta, G. Roman, A.W. Kazimiera, Preparation and characterization of sodium alginate/chitosan microparticles containing esculin, Colloids Surf. A Physicochem. Eng. Asp. 510 (2016) 22–32, https://doi.org/10.1016/j.colsurfa.2016.08.029.

[60] L. Jie, Y.P. Zhang, M. Zarei, L. Zhu, J.O. Sierra, P.M. Mertz, S.C. Davis, A topical aqueous oxygen emulsion stimulates granulation tissue formation in a porcine second-degree burn wound, Burns 41 (5) (2015) 1049–1057, https://doi.org/10.1016/j.burns.2014.11.016.

[61] X. Yang, L. Yuan, C. Xiong, C. Yin, J. Ruan, Abacopteris penangiana exerts testosterone-induced benign prostatic hyperplasia protective effect through regulating inflammatory responses, reducing oxidative stress and anti-proliferative, J. Ethnopharmacol. 157 (2014) 105–113, https://doi.org/10.1016/j.jep.2014.09.025.

[62] A.B. Shekhter, T.G. Rudenko, L.P. Istranov, A.E. Guller, R.R. Borodulin, A.F. Vanin, Dinitrosyl iron complexes with glutathione incorporated into a collagen matrix as a base for the design of drugs accelerating skin wound healing, Eur. J. Pharmaceut. Sci. 78 (2015) 8–18, https://doi.org/10.1016/j.ejps.2015.06.002.

[63] J. Boateng, O. Catanzano, Advanced therapeutic dressings for effective wound healing–a review, J. Pharm. Sci. 104 (11) (2015) 3653–3680, https://doi.org/10.1002/jps.24610.

[64] S.I. Okizaki, Y. Ito, K. Hosono, K. Oba, H. Ohkubo, H. Amano, M. Shichiri, M. Majima, Suppressed recruitment of alternatively activated macrophages reduces TGF-β1 and impairs wound healing in streptozotocin-induced diabetic mice, Biomed. Pharmacother. 70 (2015) 317–325, https://doi.org/10.1016/j.biopha.2014.10.020.

[65] E. Rizzi, M.M. Castro, C.S. Ceron, E.M. Neto-Neves, C.M. Prado, M.A. Rossi, J. E. Tanus-Santos, R.F. Gerlach, Tempol inhibits TGF-β and MMPs upregulation and prevents cardiac hypertensive changes, Int. J. Cardiol. 165 (1) (2013) 165–173, https://doi.org/10.1016/j.ijcard.2011.08.060.

[66] R. Xie, W. Zheng, L. Guan, Y. Ai, Q. Liang, Engineering of hydrogel materials with perfusable microchannels for building vascularized tissues, Small 16 (15) (2020), e1902838, https://doi.org/10.1002/smll.201902838.

[67] J. Wu, K. Zheng, X. Huang, J. Liu, H. Liu, A.R. Boccaccini, Y. Wan, X. Guo, Z. Shao, Thermally triggered injectable chitosan/silk fibroin/bioactive glass nanoparticle hydrogels for in-situ bone formation in rat calvarial bone defects, Acta Biomater. 91 (2019) 60–71, https://doi.org/10.1016/j.actbio.2019.04.023.

[68] T. Kageyama, T. Kakegawa, T. Osaki, J. Enomoto, T. Ito, T. Nittami, J. Fukuda, Rapid engineering of endothelial cell-lined vascular-like structures in in situ crosslinkable hydrogels, Biofabrication 6 (2) (2014), 025006, https://doi.org/10.1088/1758-5082/6/2/025006.